

Accepted Manuscript

Numerical study of contact forces for crack closure analysis

F.V. Antunes, A.G. Chegini, L. Correia, R. Branco

PII: S0020-7683(13)00507-6

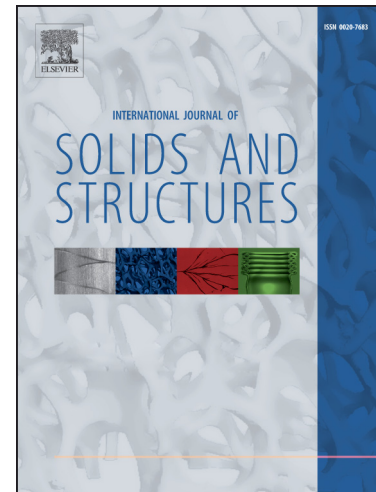
DOI: <http://dx.doi.org/10.1016/j.ijsolstr.2013.12.026>

Reference: SAS 8229

To appear in: *International Journal of Solids and Structures*

Received Date: 6 September 2013

Revised Date: 13 December 2013



Please cite this article as: Antunes, F.V., Chegini, A.G., Correia, L., Branco, R., Numerical study of contact forces for crack closure analysis, *International Journal of Solids and Structures* (2013), doi: <http://dx.doi.org/10.1016/j.ijsolstr.2013.12.026>

This is a PDF file of an unedited manuscript that has been accepted for publication. As a service to our customers we are providing this early version of the manuscript. The manuscript will undergo copyediting, typesetting, and review of the resulting proof before it is published in its final form. Please note that during the production process errors may be discovered which could affect the content, and all legal disclaimers that apply to the journal pertain.

Numerical study of contact forces for crack closure analysis

FV Antunes^{*1}, AG Chegini¹, L Correia², R Branco³

¹) CEMUC, Department of Mechanical Engineering, University of Coimbra
Rua Luís Reis Santos, Pinhal de Marrocos, 3030-788 Coimbra, Portugal

²) CEMUC, Escola Superior de Tecnologia do Instituto Politécnico de Castelo Branco
Av. do Empresário, 6000 - 767 Castelo Branco

³) Polytechnic Institute of Coimbra, ISEC, Department of Mechanical Engineering, Coimbra, Portugal

Abstract

Plasticity induced crack closure (PICC) has been widely studied using numerical models. Different numerical parameters can be considered to quantify the opening level, namely one based on the analysis of contact stresses at minimum load. A modified version of this parameter is proposed here, based on nodal contact forces instead of contact stresses. The predictions were found to be similar to those obtained from the contact status of 2nd node behind crack tip. The PICC_{contact} parameter was also found to be very consistent and adequate for parametric studies of the influence of different physical parameters. The contributions to the opening stress intensity factor of different points along crack flank were found to strongly decrease with distance to crack tip. The cumulative K_{open} between the crack tip and a distance of 0.1 mm was found to vary from 30% to 100%, increasing with stress ratio, R . Finally, a K solution was developed for punctual forces applied on crack flank and compared with a literature solution for infinite plates. A good agreement was found for plane strain state but significant differences of about 10% were found for plane stress state.

Keywords plasticity induced crack closure; contact forces, contact stress method, remote compliance

* Corresponding author. Tel.: 351-239-790700; Fax 351-239-790701; E-mail: fernando.ventura@dem.uc.pt

1. Introduction

Crack closure, i.e., the contact of fracture surfaces, affects the fatigue crack growth rate and must be considered in the design of components submitted to cycling loading. Plasticity induced crack closure (PICC) is linked to the residual plastic field formed as the crack propagates. The deformed material acts as a wedge behind the crack tip and the contact of fracture surfaces is forced by the elastically deformed material recovering its position during unloading (Elber, 1970, 1971). Numerical models based on finite element method have been successfully developed to predict PICC. These models comprise the modelling of the cracked body with elastic-plastic behaviour, the application of a cyclic load, the extension of the crack and the measurement of crack closure level. The procedure is ideal for parametric studies about the influence of physical parameters like stress ratio (R), overload ratio, crack length or material hardening parameters. Main numerical parameters are the finite element mesh (particularly the size of crack tip elements), the number of load cycles between crack increments, the crack propagation required to stabilise PICC, and the parameter considered to quantify PICC.

Although the large number of studies already developed to optimise the numerical models devoted to PICC, there are some unsolved issues. The parameter considered in the numerical studies to quantify the level of PICC has a major influence on the predictions, therefore deserves a particular attention. Different PICC numerical parameters have been considered, namely, the last contact of nodes behind crack tip, the stress inversion at the crack tip, the variation of compliance measured at a remote position relatively to crack tip, and the PICC based on the contact stresses at minimum load. The last contact of crack flank, which corresponds to the contact of first node behind current crack tip, was first used by Newman (1976) and is the most popular approach (Fleck 1986; McClung

and Sehitoglu, 1989; Solanki, 2004a; Jiang, 2005). The opening stresses are found when the displacement of the monitored node becomes positive during the loading stage of a load cycle and the closing stresses are found when the displacement of this node is zero during the unloading stage. Alternatively, the second node behind crack tip has also been used (Pommier, 2001; Roychowdhury and Dodds, 2003a). This second node may be expected to be less influenced by finite element errors associated with the severe near crack tip gradients. However, the results from both nodes are mesh dependent, since the approximation of the node to the crack tip with mesh refinement increases the opening load. An alternative parameter is the stress inversion at the crack tip, first used by Sehitoglu and Sun (1991) and followed by Wu and Ellyin (1996), González-Herrera and Zapatero (2005) and Matos and Nowell (2007). Initially the opening stress was defined as the remote stress for which all the compressive stresses along the crack plane were overcome. In a later work Sun and Sehitoglu (1992) defined crack opening stress as the external applied stress for which the stress at the crack tip node changes from compressive to tensile. When the size of crack tip element tends to zero, the contact status and the tip tension are expected to give the same result (Antunes and Rodrigues, 2008). However, important differences in the crack closure levels were obtained between classical definition and stress inversion for typical element sizes (Antunes and Rodrigues, 2008; Wei and James, 2000). Global measurements of PICC based on the analysis of remote change have also been considered numerically (Antunes 2010) replicating an experimental approach widely used (Borrego, 2001). This parameter overcomes the limitation of focusing attention on a single node, considering instead the global behaviour of the entire crack surface, however it cannot be used to obtain the distribution of PICC along a 3D crack front. An alternative approach is the contact stress method, which uses the contact stresses at minimum load to calculate the stress intensity factor required to

open the crack (Solanki, 2004b). This method also involves several nodes along crack flank and can be used to quantify PICC distribution along a 3D crack front. However, it is based on elastic analysis and may not apply to cases where the small scale yielding conditions do not hold.

There is no agreement in the literature about which parameter effectively expresses the effect of crack closure on fatigue crack growth. Borrego *et al.* (2003, 2004, 2005) used a small pin-gauge placed at the centre of a M(T) specimen to obtain the compliance curve (Toyosada and Niwa, 1994) and the technique known as maximisation of the correlation coefficient (Allison, 1988) to identify the crack closure load. The resulting crack closure levels were able to explain the influence of stress ratio, overloads and load blocks on fatigue crack growth rate in aluminium alloys. Zapatero *et al.* (2008) developed experimental and numerical work to identify the most adequate PICC parameter. CT specimens with thicknesses of 4, 8 and 12 mm were tested under constant amplitude loading with $R=0.1, 0.3, 0.5$ and 0.7 . Several definitions of effective stress intensity factor range, $\Delta K_{\text{eff}}=U\Delta K$ were tried in plane stress and plane strain states, using different parameters to quantify U , namely, node contact, tip tension and opening/closure. Best correlation coefficients were obtained for plane stress state from averaging the loading and unloading values of PICC obtained from tip tension and node contact. Further work is clearly necessary to objectively identify the PICC parameter that is effectively controlling crack tip fields and crack propagation. Comparisons between different PICC parameters can be found in Solanki *et al.* (2004b), Matos and Nowell (2007), Antunes and Rodrigues (2008) and Ismonov and Daniewicz (2010). However, Antunes and Rodrigues (2008) did not include the analysis of contact stresses, and the other studies used relatively simple material models. In fact, Solanki *et al.* (2004b) and Matos and Nowell (2007) considered an elastic-perfect plastic behaviour, while Ismonov

and Daniewicz (2010) used a bilinear kinematic hardening. Considering the relevance of PICC parameter on numerical predictions, further comparisons are important, particularly for relatively complex material models.

The contact forces have also been used to analyse different aspects of PICC phenomenon. Hou and Charng (1996) studied the effect of crack propagation on residual stresses in the presence of overloads, Hou (2004) compared the surface and deepest point of a surface crack at $R=0$ and $R=-1$, while Zhao *et al.* (2004) compared plane stress and plane strain states. Roychowdhury and Dodds (2003b) studied the variation of closure along the thickness in a through-thickness geometry, Zhang *et al.* (1999) used the contact forces to study the effect of an overload, Matos and Nowell (2008) studied the effect of crack propagation and number of load cycles between propagation and Singh *et al.* (2008) analysed the progressive contact of elements behind crack tip.

The contact stress method has not been widely used to quantify PICC and further work is required with different material models and loading parameters to check its robustness. Therefore, the main objective here is to explore the use of contact forces to analyse plasticity induced crack closure. The approach proposed by Solanki *et al.* (2004b) and Matos and Nowell (2007) to calculate the opening stress is slightly modified by considering only the nodal forces, instead of the stress distribution along crack flank. The corresponding PICC parameter is compared with classical solutions, namely the contact status of first and second nodes behind crack tip and the variation of remote compliance. This comparison is made for a wide range of load parameters and a relatively complex material hardening model. A numerical K solution is also developed for punctual loads applied at the crack flanks, and compared with Isida's solution for cracks in an infinite plate (Tada, 2000).

2. Numerical procedure

Figure 1a illustrates the geometry of Middle-Tension (M(T)) specimen studied here, which is in agreement with ASTM E647 standard (2011). Due to the symmetry of the sample and loading conditions, only 1/8 of the MT specimen was simulated, by using adequate boundary conditions. The opposite crack surface was simulated by assuming frictionless contact conditions over a symmetry plane placed behind the growing crack front. A straight crack was modelled, with an initial size a_0 of 5 mm ($a_0/W=0.083$). Pure plane strain conditions were simulated constraining out of plane deformation in a specimen with a small thickness ($t=0.1$ mm). All the simulations were performed assuming a constant amplitude cyclic loading. Table 1 indicates the load parameters defined in the five sets of constant amplitude tests considered. Sets with constant K_{min} , K_{min} , ΔK and R were studied, as can be seen.

The material considered in this research was the 6016-T4 aluminium alloy (HV0.5=92). Since PICC is a plastic deformation based phenomenon, the hardening behaviour of the material was carefully modelled. In the present work, an anisotropic yield criterion (Hill, 1948) was considered, which is expressed by the quadratic function:

$$F(\sigma_{yy} - \sigma_{zz})^2 + G(\sigma_{zz} - \sigma_{xx})^2 + H(\sigma_{xx} - \sigma_{yy})^2 + 2L\tau_{yz}^2 + 2M\tau_{zx}^2 + 2N\tau_{xy}^2 = 1 \quad (1)$$

where σ_{xx} , σ_{yy} , σ_{zz} , τ_{xy} , τ_{xz} and τ_{yz} are the components of the effective stress tensor ($\boldsymbol{\sigma}' - \mathbf{X}$) defined in the orthotropic frame and F , G , H , L , M , N , are coefficients that characterise the anisotropy of the material. In order to model the hardening behaviour of this aluminium alloy, three types of mechanical tests have been performed: uniaxial tensile tests and monotonic and Bauschinger shear tests. From the experimental data and curve fitting results, for different constitutive models, it was determined that the

mechanical behaviour of this alloy is better represented using an isotropic hardening model described by a Voce type equation:

$$Y = Y_0 + R_{\text{sat}} (1 - e^{-n_v \bar{\epsilon}^p}) \quad (2)$$

combined with a non-linear kinematic hardening model described by a saturation law:

$$\dot{\mathbf{X}} = C_x \left[X_{\text{sat}} \frac{\boldsymbol{\sigma}(-\mathbf{X})}{\bar{\sigma}} - \mathbf{X} \right] \dot{\bar{\epsilon}}^p \quad (3)$$

In these equations Y is the equivalent flow stress, $\bar{\epsilon}^p$ is the equivalent plastic strain, Y_0 is the initial yield stress, R_{sat} is the saturation stress, n_v , C_x and X_{sat} are material constants, $\boldsymbol{\sigma}$ is the deviatoric stress tensor, \mathbf{X} is the back stress tensor, and $\dot{\bar{\epsilon}}^p$ is the equivalent plastic strain rate. The material constants determined for the batch of material in study, that were used in the numerical simulations, are: $F=0.5998$; $G=0.5862$; $H=0.4138$; $L=1.2654$; $M=1.2654$; $N=1.2654$, $Y_0=124$ MPa, $R_{\text{sat}}=291$ MPa, $n_v=9.5$, $C_x=146.5$ and $X_{\text{sat}}=34.90$ MPa (Chaparro, 2008).

Figure 2 presents the finite element mesh, which was refined at the crack front to model the severe plastic deformation gradients and enlarged at remote positions to reduce the numerical effort. Three sizes were considered for the near crack tip elements, $L_1=32$; 16 or 8 μm , while only one layer of elements was considered along the thickness. The total number of linear isoparametric elements were 1275, 2587 and 12632, respectively, while the number of nodes was 2712, 5382 and 6169, respectively. The coordinate system considered to define the numerical model is indicated in figure 2. Crack propagation was simulated by successive debonding of nodes at minimum load. The increment at minimum load was adopted to overcome convergence difficulties. Each crack increment (Δa_i) corresponded to one finite element and two load cycles were applied between increments. In each cycle, the crack propagates uniformly over the thickness by releasing both current crack front nodes. Total crack increments of 0.96 mm

were considered, which correspond to 30, 60 and 120 crack propagations for meshes with $L_1=32$; 16 or 8 μm , respectively.

The opening load, F_{op} , necessary for the determination of the closure level was determined considering three approaches. The first consisted in evaluating the contact status of the first nodes behind the current crack tip with the symmetry plane. In order to avoid resolution problems associated with the discrete character of load increase, the opening load was obtained from the linear extrapolation of the applied loads corresponding to two increments after opening. The second approach was a global method (Toyosada and Niwa, 1994) based on the analysis of the global compliance data captured at the centre of the specimen. From the load-displacement records, variations of P_{op} were derived using the maximisation of the correlation coefficient technique (Allison, 1988). This technique involves taking the upper part of the $F-\varepsilon$ data and calculating the least squares correlation coefficient. The next data pair is then added and the correlation coefficient is again computed. The procedure is repeated for the whole data set. The point at which the correlation coefficient reaches a maximum could then be defined as F_{op} (Borrego, 2003). The third approach is based on the contact forces at minimum load and will be described in detail in next section.

The numerical simulations were performed with the Three-Dimensional Elasto-plastic Finite Element program (DD3IMP) that follows a fully implicit time integration scheme (Menezes and Teodosiu, 2000). The mechanical model and the numerical methods used in the finite element code DD3IMP, specially developed for the numerical simulation of metal forming processes, take into account the large elastic-plastic strains and rotations that are associated with large deformation processes. However, the isoparametric elements have a deficient behaviour when used to solve elastic-plastic problems, since the full integration scheme causes the appearance of artificial hydrostatic

stresses. To avoid the locking effect a selective reduced integration method is used in DD3IMP (Alves and Menezes, 2003; 2001). The optimum values of the numerical parameters of the DD3IMP implicit algorithm have been well established in previous works, concerning the numerical simulation of sheet metal forming processes (Oliveira and Menezes, 2004) and PICC (Antunes and Rodrigues, 2008).

Figure 3a presents the stress-strain curve σ_{yy} - ε_{yy} registered at a Gauss point (GP) during crack propagation. The stresses were normalized by the yield stress of the aluminium alloy (124.2 MPa). Figure 3b shows the Gauss point and the successive positions of crack tip. Although the initial distance between the GP and the crack tip, the first loading produces plastic deformation, which indicates that the GP is within the first forward plastic zone. A compressive stress state is observed at minimum load but no reversed plasticity occurs. As the crack propagates the GP approaches the crack tip, and the stress level increases producing more plastic deformation. The compressive stress at minimum load also increases and starts producing reversed plastic deformation. The maximum plastic deformation happens when the GP is immediately ahead of crack tip, i.e., when the crack tip is at position 29 in figure 3b. The two load cycles applied between crack propagation are now clearly visible, and the stress level reaches about 3 times material's yield stress as a consequence of isotropic hardening. When the crack moves ahead of the GP (crack tip at position 30 in figure 3b), the stress level applied to the GP becomes relatively low and the plastic deformation ceases. The plastic deformation is now a residual deformation.

3. Contact stress method

At minimum load, residual compressive stresses exist along the crack flanks. This residual stresses can be used to calculate a negative residual stress intensity factor (K_{res}).

This does not have physical sense, but by employing a superposition argument it may be used to calculate the opening stress intensity factor, K_{open} , needed to overcome the residual stress field and open the entire crack. The contact forces are obtained at minimum load, therefore the opening level is given by (Matos and Nowell, 2007):

$$K_{open}=K_{min}+K_{res} \quad (4)$$

It is assumed that only elastic deformation takes place until the crack opens. The contact stress method has advantages, namely, it involves several nodes instead of focusing on a single node; it is expected to be less affected by finite element errors since it does not study only near crack tip nodes; and no extrapolation is needed which avoids resolution problems associated with discrete load increments (Solanki, 2004b).

Dill and Saff (1976) were the first to introduce a contact stress method to compute crack opening loads, and employed the methodology in a strip-yield model. Newman (1981) has long employed this method within the strip yield model Fastran. Solanki *et al.* (2004b) for the first time applied the method to finite element analysis. They considered analytical expressions of K for infinite plates and applied the methodology to CT and M(T) specimens. Matos and Nowell (2007) used the weight function method introduced by Bueckner (1970) to calculate the residual stress intensity factor. In both studies a linear variation of stresses was assumed along each finite element. The opening results were compared with values from the contact at first and second nodes behind crack tip. The contact stress method gave higher predictions than the first node behind crack tip.

A solution for a crack in an infinite plate submitted to pairs of punctual forces on the crack flank can be found in literature, proposed by Isida (Tada, 2000). However, considering the finite size of the M(T) specimen it was decided to develop a new solution. A relation between a punctual contact force and its distance to crack tip (d) was therefore defined here numerically using the finite element method. A mesh with 1

μm elements at the crack front was considered in a linear elastic analysis and K was calculated from J integral. A direct method based on the extrapolation of K values obtained from crack opening displacements was also considered to validate the J integral results. The punctual load imposed difficulties to the numerical calculation of J , particularly for small values of distance d . The path of J integral must lie between the load and the crack tip, therefore a quite refined mesh is required. Non-dimensional parameters were defined as:

$$K^* = \frac{K}{F_p / (t \cdot W) \sqrt{W}} \quad (5)$$

$$d^* = \frac{d}{W} \quad (6)$$

where F_p is the punctual force, d is its distance to crack tip, t and W are the thickness and the width of the $M(T)$ specimen, respectively. Figure 4 shows the results of K^* versus d^* for plane stress and plane strain states, which were found to be independent of crack length ($2a$) at least for values of a in the range 5-7.5 mm. The stress intensity factor presents an asymptotic behavior, increasing to infinity when the punctual force approaches the crack tip. For relatively large distances the resulting stress intensity factor approaches zero, as could be expected. The stress state produced a relatively low influence on K . A numerical model with two fitting constant was applied to the results of figure 4:

$$K^* = \frac{C_1}{(d^*)^{C_2}} \quad (7)$$

Fitting difficulties were observed for the values remote to the crack tip, therefore d^* was divided into 2 regions, as indicated in figure 4 by the vertical dashed line. Table 2 presents the ranges of d^* and respective fitting constants, which were obtained by regression analysis using the optimisation tools of Excel. For d/W lower than 0.012, the

average of absolute differences are less than 0.5% for both plane stress and plane strain states. As can be seen in table 2, near the crack tip C_2 is close to 0.5, which is according to Isida's solution ($K = \sqrt{2/(\pi d)}F_c$). The results of figure 4 were compared with this literature solution and a good agreement was found for plane strain state and small distances of the punctual force relatively to the crack tip. On the other hand, significant differences of about 10% were found for plane stress state, which justify the need for the solution developed here.

The model based on equation 7 was applied to obtain individual crack opening levels for each contact force along crack front. The total residual stress intensity factor was finally found by summing the contributions from the individual nodes in contact. The linear superposition is assumed to be valid, which was demonstrated in previous work (Antunes 2013, in press). Notice that in Solanki's proposal a linear stress distribution is assumed across each finite element along the crack flank, while in here only the nodal forces are used to predict the crack opening values. This is interesting since the nodal forces are primary outputs of the finite element method, while the stresses are obtained by extrapolation from the Gauss points.

4. Numerical results

4.1. Contact forces and K distribution

Figure 5 shows typical distributions of contact stresses at minimum stress versus distance to crack tip, d . These forces are a first order output of the elastic-plastic FEM analysis, and the smooth variations observed are a good indication for the accuracy. The contact stresses obtained by Solanki *et al.* (2004b) were more irregular which can be explained by the extrapolation required to obtain the nodal stresses from Gauss points values. The contact extends over the entire crack flank submitted to crack propagation,

with a non uniform distribution of contact forces. The nodes closest to crack tip have the largest contact forces, as could be expected. For plane stress state a sharp decrease is observed up to about $d=0.25$ mm, and for distances to crack tip greater than 0.25 mm the variation is relatively small. For plane strain state the contact stresses are significantly lower, as was expected. In fact, there is a general agreement in literature about the relatively low PICC level observed under plane strain conditions. For plane strain state the contact is observed not only immediately behind current crack tip, but also at the position corresponding to the beginning of crack propagation. This remote contact is explained by the relatively high plastic deformation observed in plane strain state at the first load cycles. Fleck (1986) also indicated that a residual wedge of material is left at a location immediately ahead of initial location of crack tip, which leads to discontinuous crack closure (first contact of crack flanks at a position remote from current crack tip).

Figure 6 shows the effect of crack propagation on nodal contact forces for plane stress state (open symbols) and plane strain state (filled symbols). For plane stress state, as the crack propagates more nodes have contact forces. Immediately behind the crack tip the contact forces do not vary significantly with crack propagation. The extent of the region with contact forces is, for constant amplitude loading, only related with the extent of numerical crack propagation. However, as will be seen next, only the contact near the crack tip contributes significantly to the crack opening level. The peak of contact forces corresponding to the beginning of crack propagation, evident for plane strain state, is also observed for plane stress state in this plot.

Figure 7 shows the contributions to the opening stress intensity factor of different points along crack flank. There is a strong decrease from the crack tip, more pronounced than observed for the variation of contact stresses along crack flank. In fact, the stress intensity factor decreases substantially with distance d from crack tip, as equation 7

expresses. Additionally, the contact forces at minimum load decrease substantially from crack tip, as figures 5 and 6 illustrate. These two effects, i.e., the decrease of contact forces and of their influence with distance to crack tip, explain the variation of PICC observed in figure 7. The dashed line was obtained for plane stress state considering that the contact stress is constant along crack flank ($\sigma_{\text{contact}}=186$ MPa). The difference relatively to the plane stress set (filled circles) expresses the effect of force variation along crack flank. A power-type curve was fitted by regression to the plane stress results, showing that there is an exponential decrease from crack tip. For plane stress state, the exponent obtained (-0.928) is significantly higher, in absolute terms, than obtained for the dashed line, i.e., for the iso-stress curve which is about -0.5.

The contact forces method is very interesting to understand and quantify how closure develops behind crack tip. Figure 8 shows the cumulative stress intensity factor along the crack flank, from the crack tip up to a distance d_{max} . Two curves of cumulative K are presented for d_{max} of 0.1 or 0.2 mm. The cumulative K varies significantly from about 30% to 100%, depending on stress ratio, R . For stress ratios lower than zero, the distribution is not so concentrated near the crack tip and the effect of R is moderate. On the other hand, for R higher than zero the increase of stress ratio produces a rapid increase of closure near crack tip. For relatively high R there is a strong concentration of closure immediately behind the crack tip, i.e., the contact only happens immediately behind crack tip. Solanki *et al.* (2004b) analysed the contribution of the first element behind crack tip to the total opening value and also found significant values at $R=0$, namely for the CT specimen under plane strain state.

4.2. Comparison of PICC parameters

Figure 9 shows the variation of crack opening level with crack propagation, Δa , obtained with the contact stress method, with the remote compliance technique and with the analysis of contact status of first, second and third nodes behind crack tip (nodes 1, 2 and 3 respectively). For plane stress state all the PICC parameters, including the one based on the contact forces, show a strong increase of closure at the beginning of crack propagation, and a stabilised behaviour afterwards. In numerical studies some crack propagation is always required to built the residual plastic wake and obtain stabilised opening values. $PICC_{\text{contact}}$ is lower than the value obtained from node 1, higher than the value obtained from compliance analysis and node 3, and similar to node 2 predictions. For plane strain state the level of PICC is significantly lower compared with the plane stress state, but the effect of PICC parameters was found to be similar. A peak was observed at the beginning of crack propagation which is explained by the significant plastic deformation occurring at the first load cycles, which is evident in the contact stresses presented in figure 5. With propagation the crack tip moves away from the plastic wedge and its influence on PICC attenuates progressively.

Figure 10 compares $PICC_{\text{contact}}$ with the other parameters for the load conditions presented in table 1, and the trends observed in figure 9 are confirmed. The predictions obtained from the analysis of contact status of node 2 behind crack tip are always similar to those obtained with the contact forces, the remote compliance gives lower opening values and the node 1 gives higher values. Note that 2nd node method and the contact stress method are quite distinct approaches and the coincidence of results cannot be easily explained. The values obtained by Solanki *et al.* (2004) and Matos and Nowell (2007) with the contact stresses were higher than those obtained with the first node behind crack tip. However, notice that they assumed a linear distribution of stresses in each element along crack flank, while in here only the nodal forces are used. The contact

stresses between the crack tip and the first node behind it have significant a contribution to the K opening value, which is not considered here. Roychowdhury and Dodds (2003b) suggested that node 1 closes prematurely and exhibits opening loads much higher than the other nodes, therefore they used the second node behind crack tip. The detailed analysis of the effect of the different loading parameters indicated in table 1 showed that the $PICC_{\text{contact}}$ is a consistent parameter, giving the same trends than observed with other parameters namely the well-established node 1 parameter. Further work is however necessary to understand which parameter is effectively adequate to quantify the effect of crack closure on fatigue crack growth rate.

4.3. Effect of PICC variation on fatigue life

The effect of PICC variations, shown in figures 9 and 10, on fatigue life was analysed in a parallel study. Fatigue crack propagation was simulated using a fully automatic three-dimensional finite element technique (Lin and Smith, 1999). This technique comprises five main steps cyclically repeated, i.e. definition of a numerical model representative of the cracked body; calculation of the displacement field; determination of the SIF values at the crack front nodes; computation of the crack front advances by applying experimental $da/dN-\Delta K$ results; and optimization of the new crack front by applying a cubic spline. Detailed information about the technique can be found elsewhere (Lin and Smith, 1999).

The geometry analyzed was the M(T) specimen. The cracks were assumed to be planar, normal to the longitudinal axis of the specimen and existing in its middle-section. Three different thicknesses were studied, namely $2t=15$, 20 and 25mm. Due to symmetries in terms of geometry, material and loading, only one-eighth of the specimen was modelled ($W=25$ mm, $L=100$ mm). The initial crack was straight and with a length

$a_0/W=0.06$. A constant amplitude cyclic loading was applied with $\sigma_{\max}=50$ MPa and $R=0$. The material simulated was the 6016-T4 aluminium alloy, which was defined as homogeneous, isotropic and linear elastic ($E=70$ GPa and $\nu=0.33$). The constants of the Paris law ($C=1.45 \times 10^{-11}$ and $m=3.4$) were obtained experimentally (Antunes, 2010) from $da/dN-\Delta K$ results (da/dN in m/cycle and ΔK in $\text{MPa}\cdot\text{m}^{1/2}$). A detailed description of finite element mesh, which had 35,070 nodes and 2,625 elements can be found elsewhere (Branco and Antunes, 2008). The mesh was created using isoparametric hexahedric elements with 20 nodes and isoparametric pentahedric elements with 15 nodes. Singular pentahedric elements with nodes at quarter-point positions were used along crack front. Crack closure was introduced into the fatigue crack growth simulation considering effective stress intensity factor ranges, i.e.:

$$\Delta K_{\text{eff},i}^{(j)} = U_i \cdot \Delta K_i^{(j)} \quad (7)$$

where $\Delta K_i^{(j)}$ is the SIF range of the i^{th} node of the j^{th} iteration and U_i is the fraction of the load cycle for which the crack remains fully open. Near the surface the values of U varied linearly from the value for plane stress state (U_A) to the value for plane strain state (U_B). In the other regions, predominantly subjected to plane strain state, the values of U were equal to U_B . The extent of surface region, S_1 , was determined applying the procedure proposed by Branco *et al.* (2012) and a value $S_1=0.1$ mm was obtained. Four different closure parameters were studied: node 1, node 2, remote compliance, and contact forces. The values considered in the propagation study are summarized in Table 3.

Figure 11 plots the fatigue life variation (N_i/N_R) for three different thicknesses. The N_R variable, termed reference fatigue life, was calculated using the values of PICC given by the remote compliance 3. The N_i variable represents the fatigue life obtained from the other PICC parameters used here. As can be seen, the method of PICC selected

has a significantly influence on the fatigue life. The fatigue life obtained with the Node 1 method is about 56-64% higher than the reference fatigue life which a relatively high discrepancy. Even in the case of the Node 2 method, the differences relatively to the reference method are notorious, about 12-17%. With regard to the contact forces method, the variations are less expressive, i.e. lower than 4%. It is also important to refer that crack closure does not affect only the fatigue life but also the crack shape. Different crack curvatures, in particular near the free surface, were observed in these simulations. These results demonstrate the importance of the crack closure values on fatigue crack growth lives.

4.4. Variable amplitude loading

Figure 12a shows the effect of overloads on nodal contact forces measured at minimum load. The vertical lines indicate the positions along the crack flank where the overloads were applied. The plastic wedge resulting from an overload produces a peak of contact forces. A shielding effect can also be observed behind the plastic wedge, i.e., there is almost no contact. For a relatively low overload ($\sigma_{ol}/\sigma_{max}=1.13$) these effects are limited to a relatively narrow region on the crack flank. The increase of the overload to $\sigma_{ol}/\sigma_{max}=1.43$ enlarged significantly the contact distance. The shielding effect is also significantly stronger and almost no contact is observed beyond the point where the overload was applied.

Fig. 12b presents PICC versus crack increment obtained with two distinct numerical parameters. Immediately after the application of the overload the level of PICC drops suddenly and then it increases over the value corresponding to constant amplitude loading. The decrease may be explained by crack tip blunting or by reversed plastic deformation, which tend to reduce PICC. The position of the peak is linked with

the plastic deformation field generated by the overload ahead of crack tip. Finally, a relatively slow convergence to the constant amplitude behaviour is observed as the crack tip moves ahead of overload position. The results obtained with the contact stress method are once again relatively low compared with those from node 1 behind crack tip.

Finally, figure 13 presents the effect of high-low and low-high load blocks on contact forces. For low-high conditions, the contact forces indicate that the region of crack faces corresponding to the initial load block simply does not contact, because the crack face corresponding to second load block has a shielding effect over it. On the other hand, for the high-low regime two peaks can be identified at the current crack tip position and at the load transition. The final low level regime has relatively low contact forces and most of contact exists in the high level regime. This discontinuous closure, i.e., the remote contact of crack flanks, has a protective effect on crack tip (Paris, 1999).

5. Conclusions

The present paper studies the use of contact forces along the crack flanks to the analysis of plasticity induced crack closure (PICC). The main conclusions are:

- A numerical solution was developed for the stress intensity factor of a M(T) specimen submitted to pairs of punctual forces at the crack flank. The solution was compared with Isida's solution for a crack in an infinite plate and significant differences were found for plane stress state which justified the solution here developed.
- Contact forces along crack flank were determined numerically at minimum load using the finite element method. Smooth variations were obtained which is a positive indication for the accuracy of the numerical model. The effect of overloads, and Low-High and High-Low load blocks was studied through the analysis of contact forces at minimum load.

- The analysis of contact forces was found to be an excellent tool to understand and quantify the distribution of closure on crack flanks. The contributions to the opening stress intensity factor of different points along crack flank strongly decrease with distance to crack tip, d . Two cumulative factors explain this variation: the decrease of contact forces and the decrease of the contribution of a contact force with distance d . The cumulative K between the crack tip and a distance of 0.1 mm was found to vary significantly from about 30% to 100%, depending on stress ratio, R . For stress ratios lower than zero, the distribution is not so concentrated near the crack tip and the effect of R variations is moderate. On the other hand, for R higher than zero there is a strong concentration of closure immediately behind the crack tip, which increases significantly with stress ratio.

- The approach proposed by Solanki *et al.* (2004) and Matos *et al.* (2007) to calculate PICC was slightly modified by considering only the nodal forces, instead of a stress distribution along crack flank. This change modified the predictions obtained from the contact method relatively to other PICC parameters. The values obtained here for a wide range of loading parameters were found to be similar to those obtained from the analysis of contact status of node 2 behind crack tip. Solanki *et al.* and Matos *et al.* got PICC values even higher than those obtained from node 1.

- A fatigue crack propagation study was developed in M(T) specimens with different thicknesses. A great sensitivity of fatigue life to PICC variations was found, which reinforces the importance of having accurate values.

- The PICC parameter based on the contact forces emerges here as an effective alternative to classical parameters like the contact status of node 1 behind crack tip, the analysis of remote compliance or the inversion of tip tension. In fact, the calculation of $PICC_{\text{contact}}$ is relatively simple, there is no need of extrapolation or refined load

increments, and it involves several nodes behind crack tip therefore is expected to be less sensitive to mesh variations. Additionally the $PICC_{\text{contact}}$ was found to be very consistent, expressing the same trends observed for node 1 when the physical and numerical parameters are changed. Anyway, further work is necessary to understand which numerical parameter can effectively be used to quantify the effect of closure on fatigue crack growth.

Acknowledgments

The authors are indebted to the Portuguese Foundation for the Science and Technology (FCT) and COMPETE program from FEDER (European Regional Development Fund) for the financial support under the Projects PTDC/EME-PME/114892/2009 and PEst-C/EME/UI0285/2013.

References

- Allison, J.E., 1988. The measurement of crack closure during fatigue crack growth. Read DT and Reeds RP, Editors, Fracture Mechanics: Eighteenth symposium, ASTM STP 945, American Society for Testing and Materials, 913–933.
- Alves, J.L., Menezes, L.F., 2001. Application of tri-linear and tri-quadratic 3-D solid FE in sheet metal forming process simulation. In: K. Mori, editors. NUMIFORM 2001, Japan, 639–644.
- Antunes, F.V., Rodrigues, DM., 2008. Numerical simulation of plasticity induced crack closure: Identification and discussion of parameters. Engng Fracture Mech 75, 3101–3120.
- Antunes, F.V., Branco, R., Costa, J.D., Rodrigues, DM., 2010. Plasticity induced crack closure in Middle-Tension specimen: Numerical versus experimental. Fatigue Fract Engng Mater Struct 33, 673–686.
- Antunes, F.V., Correia, L., Ramalho, A.L., A parameter for quantitative analysis of plasticity induced crack closure. International Journal of Fatigue, in press.
- ASTM E647, 2011. Standard test method for measurement of fatigue crack growth rates. ASTM International, West Conshohocken, PA, DOI: 10.1520/E0647-11E01
- Borrego, L.P., Ferreira, J.M., Costa, J.M., 2001. Fatigue crack growth and crack closure in an AlMgSi alloy. Fatigue Fract. Engng. Mater. Struct. 24, 255-265.
- Borrego, L.P., Ferreira, J.A.M., Pinho da Cruz, J.M., Costa, J.M., 2003. Evaluation of overload effects on fatigue crack growth and closure. Eng Fract Mech 70, 1379-1397.
- Borrego, L.F.P., Costa, J.D., Sara, S., Ferreira, J.M., 2004. Microstructure Dependent Fatigue Crack Growth in Aged Hardened Aluminium Alloys. Int J Fatigue 26, 1321-1331.

- Borrego, L.P., Costa, J.M., Ferreira, J.M., 2005. Fatigue Crack Growth in Thin Aluminium Alloy Sheets Under Loading Sequences with Periodic Overloads. *Thin Walled Structures* 43(5), 772-788.
- Branco, R., Antunes F.V., 2008. Finite element modelling and analysis of crack shape evolution in mode-I fatigue Middle-Cracked Tension specimens. *Engng Fracture Mechanics* 75, 3020-3037.
- Branco, R., Antunes, F.V., Costa J.D., 2012. Extent of surface regions near corner points of notched cracked bodies subjected to mode-I loading. *Finite Elements in Analysis and Design* 50, 147-160.
- Bueckner, H.F., 1970. A novel principle for the computation of stress intensity factors. *Z Angew Math Mech* 50, 529-45.
- Chaparro, B.M., Thuillier, S., Menezes, L.F., Manach, P.Y., Fernandes, J.V., 2008. Material parameters identification: Gradient-based, genetic and hybrid optimization algorithms. *Computational Materials Science* 44(2), 339-346.
- Dill, H.D., Saff, C.R., 1976. Spectrum crack growth prediction method based on crack surface displacement and contact analysis. *Fatigue crack growth under spectrum loads ASTM STP 595*, 306-319.
- Elber, W., 1970. Fatigue crack closure under cyclic tension. *Eng. Fracture Mechanics* 2, 37-45.
- Elber, W., 1971. The significance of fatigue crack closure under cyclic tension. *Damage tolerance in aircraft structures. ASTM STP 486 Philadelphia*, 230-242.
- Fleck, N.A., 1986. Finite element analysis of plasticity-induced crack closure under plane strain conditions. *Engng Fract Mech* 25(4), 441-449.
- Gonzalez-Herrera, A., Zapatero J., 2005. Influence of minimum element size to determine crack closure stress by the finite element method. *Eng Fract Mech* 72, 337-355.
- Hill, R., 1948. A theory of the yielding and plastic flow of anisotropic metals. *Proceedings of Mathematical, Physical and Engineering Science*, Royal Society London.
- Hou, C.-Y., Charng, J.-J., 1996. Estimation of plasticity-induced induced crack closure in a pre-existing plastic zone", *Int. J. Fatigue* 18(7), 463-474.
- Hou, C.-Y., 2008. Simultaneous simulation of closure behavior and shape development of fatigue surface cracks, *Int. Journal of Fatigue* 30, 1036-1046
- Ismonov, S., Daniewicz, S.R., 2010. Simulation and comparison of several crack closure assessment methodologies using three-dimensional finite element analysis, *Int. J. Fatigue* 32, 1322-1329.
- Jiang, Y., Feng, M., Ding F., 2005. A re-examination of plasticity-induced crack closure in fatigue crack propagation. *International Journal of Plasticity* 21, 1720-1740.
- Lin, X.B., Smith, R.A., 1999. Finite element modelling of fatigue crack growth of surface cracked plates. Part I: the numerical technique. *Engng Fracture Mechanics* 63, 503-522.
- Matos, P.F.P., Nowell, D., 2007. On the accurate assessment of crack opening and closing stresses in plasticity-induced fatigue crack closure problems", *Engng Fracture Mechanics* 74, 1579-1601,.
- Matos, P.F.P., Nowell, D., 2008. Numerical simulation of plasticity-induced fatigue crack closure with emphasis on the crack growth scheme: 2D and 3D analysis. *Engng Fracture Mechanics* 75, 2087-2114.

- McClung, R.C., Sehitoglu, H., 1989. On the finite element analysis of fatigue crack closure – 1. Basic modeling issues. *Engng Fract Mech* 33(2), 237–252.
- McClung, R.C., Sehitoglu, H., 1989. On the finite element analysis of fatigue crack closure – 2. Numerical results. *Engng Fract Mech* 33(2), 253–272.
- Menezes, L.F., Teodosiu, C., 2000. Three-Dimensional Numerical Simulation of the Deep-Drawing Process using Solid Finite Elements. *Journal of Materials Processing Technology* 97: 100-106.
- Oliveira, M.C., Menezes, L.F., 2004. Automatic correction of the time step in implicit simulations of the stamping process. *Finite Elements in Analysis and Design* 40, 1995–2010.
- Newman, Jr., J.C., 1976. A finite element analysis of fatigue crack closure. *Mechanisms of crack growth*, ASTM STP 590, 281-301.
- Newman Jr., J.C., 1981. A crack closure model for predicting fatigue crack growth under aircraft spectrum loading. *ASTM STP* 748, 53-84.
- Paris, P.C., Tada, H., Donald, J.K., 1999. Service load fatigue damage – a historical perspective”, *Int. Journal of Fatigue* 21 S35-S46.
- Pommier, S., 2001. A study of the relationship between variable level fatigue crack growth and the cyclic constitutive behaviour of steel. *International Journal of Fatigue* 23, S111-S118.
- Roychowdhury, S., Dodds, Jr. R.H., 2003a. A numerical investigation of 3-D small-scale yielding fatigue crack growth. *Engng Fracture Mech* 70, 2363-2383.
- Roychowdhury, S., Dodds, R.H., 2003b. Three-dimensional effects on fatigue crack closure in small-scale yielding regime – a finite element study. *Fatigue Fract Engng Mater Struct* 26, 663–73.
- Sehitoglu, H., Sun, W., 1991. Modelling of plane strain fatigue crack closure. *J Engng Mater Technol* 113, 31–40.
- Singh, K.D., Parry, M.R., Sinclair, I., 2008. Some issues on finite element modelling of plasticity induced crack closure due to constant amplitude loading”, *Int. Journal of Fatigue* 30 1898-1920.
- Solanki, K., Daniewicz, S.R., Newman Jr J.C., 2004a. Finite element analysis of plasticity-induced fatigue crack closure: an overview. *Eng Fract Mech* 71, 149–71.
- Solanki, K., Daniewicz, S.R., Newman Jr., J.C., 2004b. A new methodology for computing crack opening values from finite element analyses. *Engng Fracture Mech* 71, 1165-1175.
- Sun, W., Sehitoglu, H., 1992. Residual stress fields during fatigue crack growth. *Fatigue Fract Engng Mater Struct* 15(2), 115–28.
- Tada, H., Paris, P.C., Irwin, G.R., 2000. *The stress analysis of crack handbook*, ASME Press.
- Toyosada, M., Niwa, T., 1994. The significance of RPG load for fatigue crack propagation and the development of a compliance measuring system. *Int J Fract* 67, 217–230.
- Zapatero, J., Moreno, B., González-Herrera, A., 2008. Fatigue crack closure determination by means of finite element analysis. *Engng Fracture Mechanics* 75, 41-57.
- Zhang, J.Z., Halliday, M.D., Bowen, P., Poole, P., 1999. Three dimensional elastic-plastic finite element modelling of small fatigue crack growth under a single tensile overload, *Engng Fracture Mechanics* 63, 229-251.
- Zhao, L.G., Tong, J., Byrne, J., 2004. The evolution of the stress–strain field near a fatigue crack tip and plasticity-induced crack closure revisited. *Fatigue Fract Eng Mater Struct* 27, 19–29.
- Wei, L.-W., James, M.N., 2000. A study of fatigue crack closure in polycarbonate CT specimens. *Engng Fracture Mech* 66, 223-242.

Wu, J., Ellyin, F., 1996. A study of fatigue crack closure by elastic-plastic finite element for constant-amplitude loading. *Int J Fract* 82, 43–65.

ACCEPTED MANUSCRIPT

List of figures

Figure 1. Middle-cracked tension, M(T), specimen.

Figure 2. Finite element mesh. a) Frontal view. b) Detail of frontal view.

Figure 3. a) Stress-strain curve for a Gauss point; b) Location of the Gauss point relatively to the crack tip ($\sigma_{\max}=60$ MPa, $\sigma_{\min}=0$, $a_0/W=0.16$, $L_1=16$ μm , $\Delta a=30 \times 16=480$ μm).

Figure 4. Non-dimensional stress intensity factor versus distance to crack tip ($W=30$ mm).

Figure 5. Contact stresses at minimum load for plane stress and plane strain states ($\sigma_{\max}=47.5$ MPa; $\Delta K=6.5$ MPa $\cdot\text{m}^{1/2}$; $R=0.02$)

Figure 6. Contact forces at minimum load for plane stress (open symbols) and plane strain states (filled symbols), versus crack propagation ($\sigma_{\max}=47.5$ MPa; $\Delta K=6.5$ MPa $\cdot\text{m}^{1/2}$; $R=0.02$).

Figure 7. Contribution to K_{open} along crack flank ($\sigma_{\max}=47.5$ MPa; $\Delta K=6.5$ MPa $\cdot\text{m}^{1/2}$; $R=0.02$)

Figure 8. Cumulative stress intensity factor up to a distance d from crack tip (plane stress).

Figure 9. PICC versus crack increment ($L_1=8$ μm ; $\sigma_{\max}=47.5$ MPa; $\sigma_{\min}=0.83$ MPa, plane stress).

Figure 10. Comparison between different PICC parameters ($L_1=8$ μm , plane stress).

Figure 11. Comparison of fatigue lives obtained with different closure values.

Figure 12. Effect of overloads ($\text{OLR}=\sigma_{\text{ol}}/\sigma_{\max}$). a) Contact forces; b) PICC versus crack increment. (Plane stress; $L_1=8$ μm ; $\sigma_{\max}=47.5$ MPa; $R=0$)

Figure 13. Effect of load blocks on contact forces (Plane stress; $L_1=8$ μm ; $R=0.02$, $\sigma_{\max 1}=47.5$ MPa, High-low: $\sigma_{\max 2}=36.7$ MPa; Low-high: $\sigma_{\max 2}=60$ MPa)

List of tables

Table 1. Load parameters ($[\Delta K]=\text{MPa}\cdot\text{m}^{1/2}$)

Table 2. Fitting constants of K^* versus d^* (equations 5-7).

Table 3. Closure parameters used in FCG simulations.

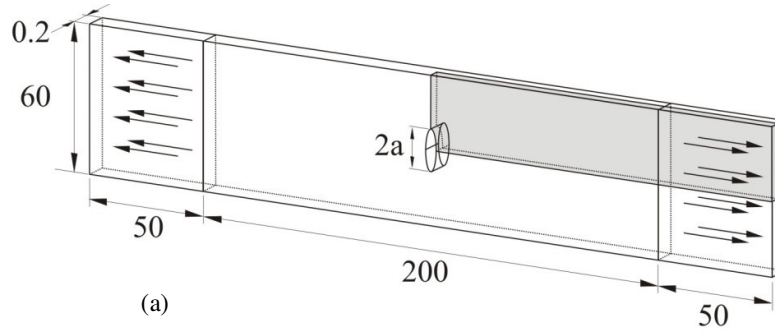


Figure 1. Middle-cracked tension, M(T), specimen.

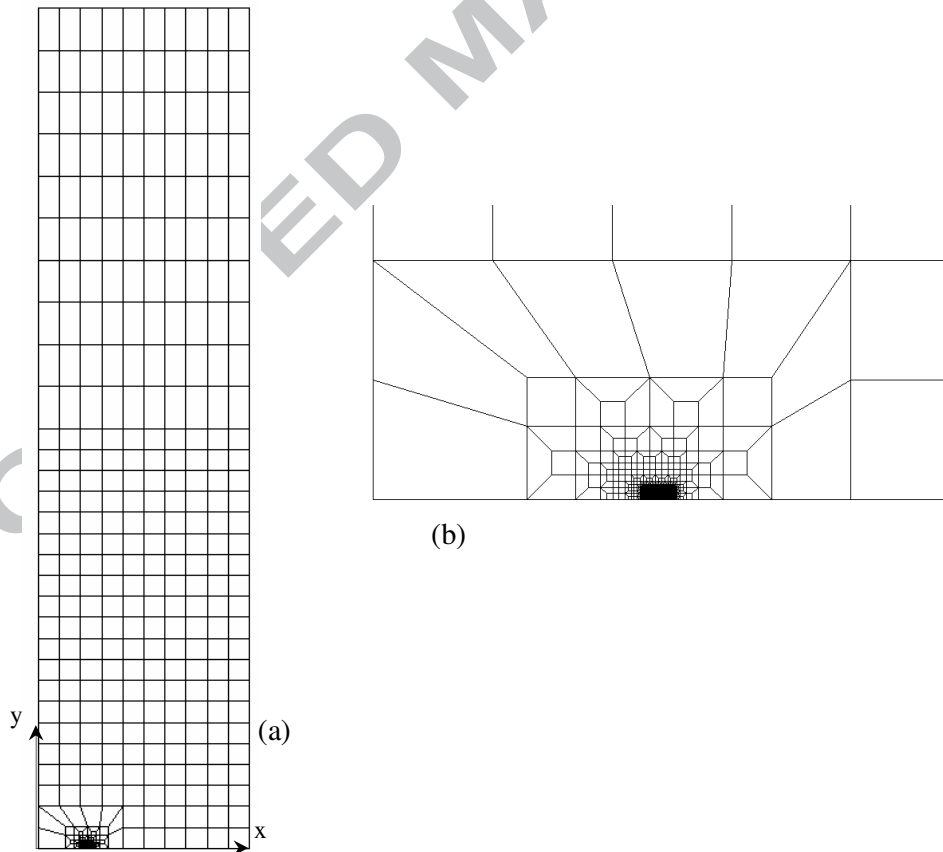


Figure 2. Finite element mesh. a) Frontal view. b) Detail of frontal view.

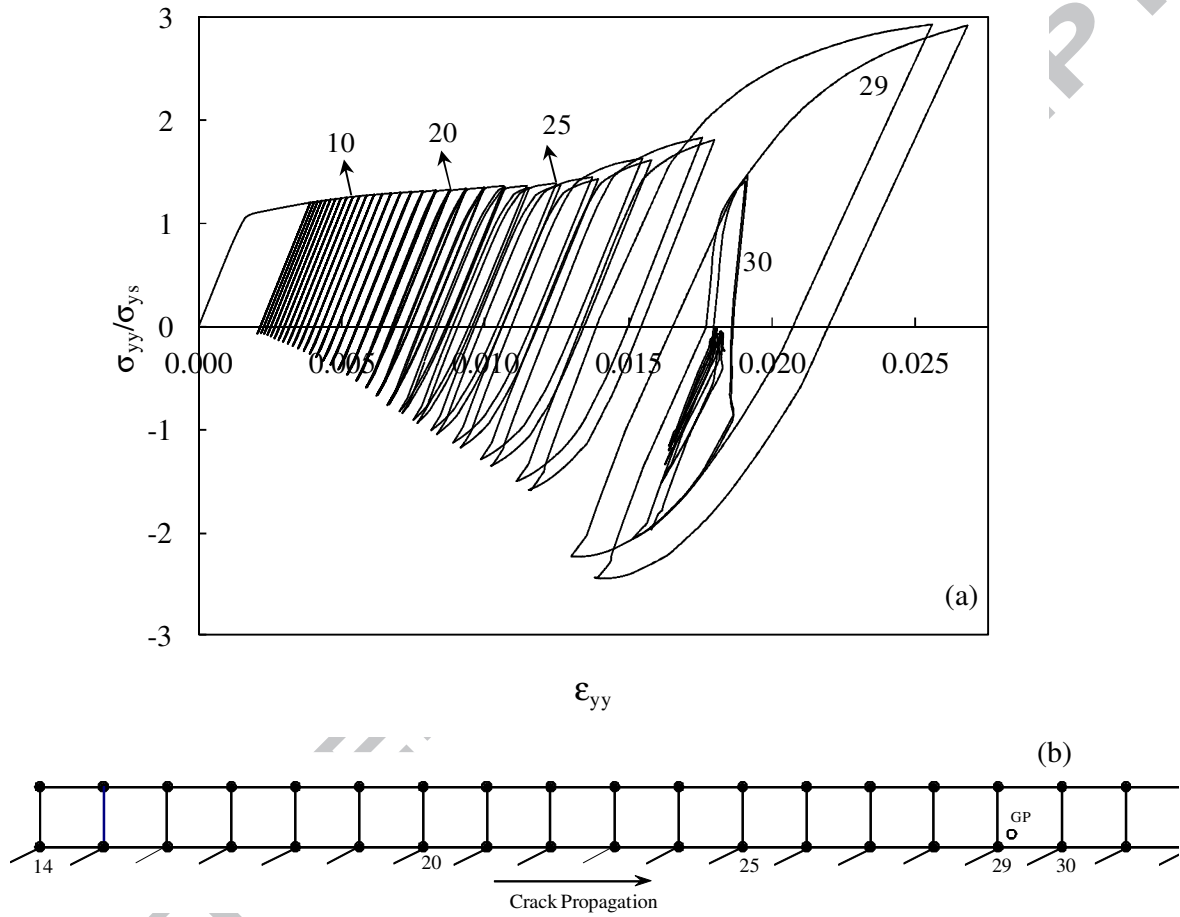


Figure 3. a) Stress-strain curve for a Gauss point; b) Location of the Gauss point relatively to the crack tip ($\sigma_{\max}=60$ MPa, $\sigma_{\min}=0$, $a_0/W=0.16$, $L_1=16$ μm , $\Delta a=30 \times 16=480$ μm).

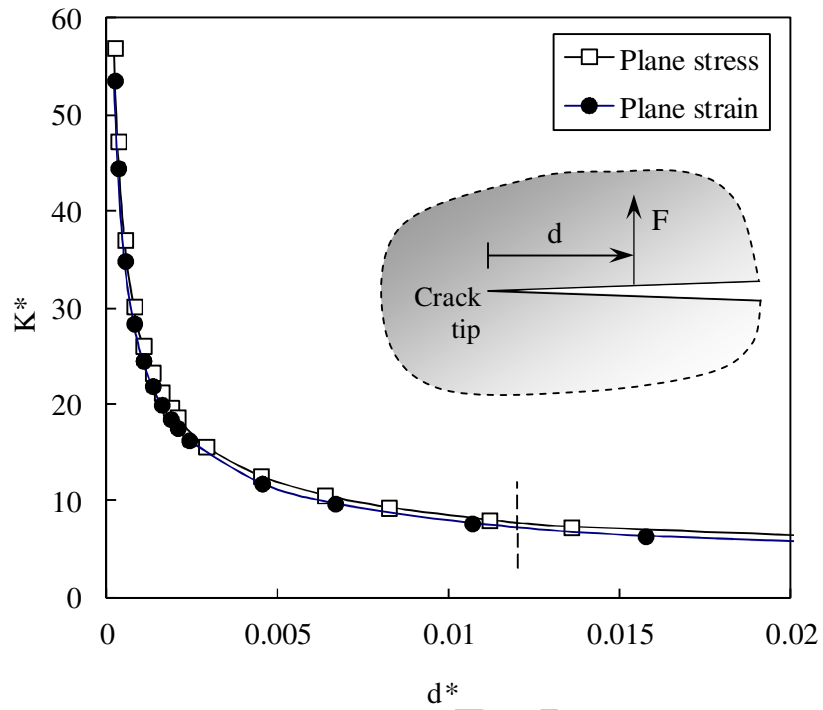


Figure 4. Non-dimensional stress intensity factor versus distance to crack tip ($W=30$ mm).

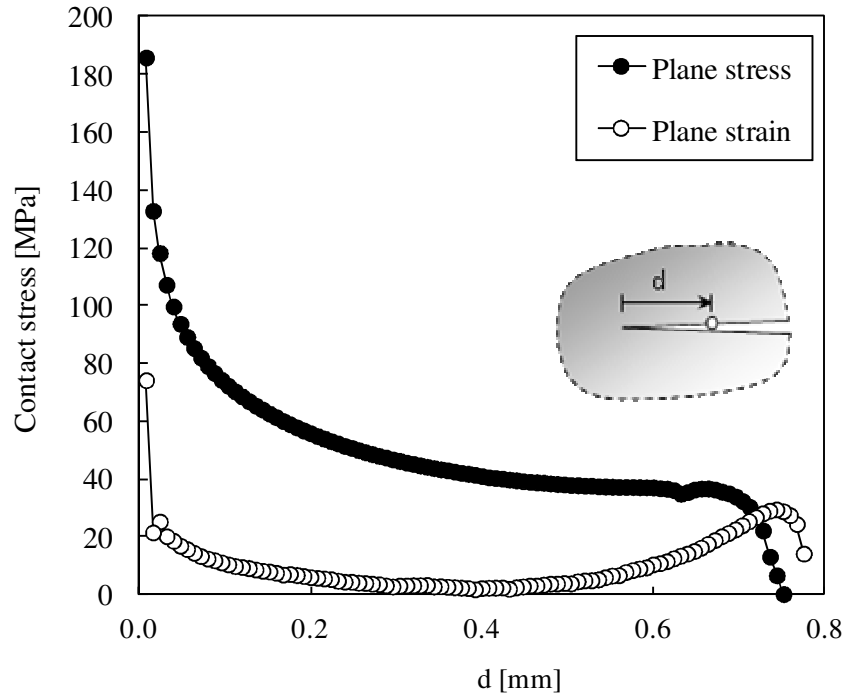


Figure 5. Contact stresses at minimum load for plane stress and plane strain states ($\sigma_{\max}=47.5$ MPa; $a=5.9$ mm, $\Delta K=6.5$ MPa \cdot m $^{1/2}$; $R=0.02$)

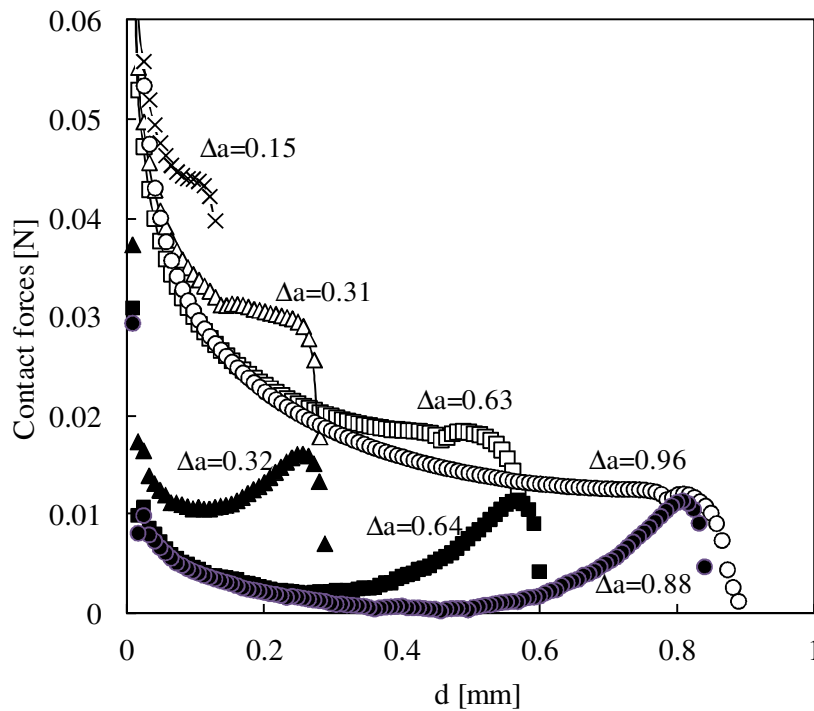


Figure 6. Contact forces at minimum load for plane stress (open symbols) and plane strain states (filled symbols), versus crack propagation ($\sigma_{\max}=47.5$ MPa; $a=5.9$ mm, $\Delta K=6.5$ MPa \cdot m $^{1/2}$; $R=0.02$).

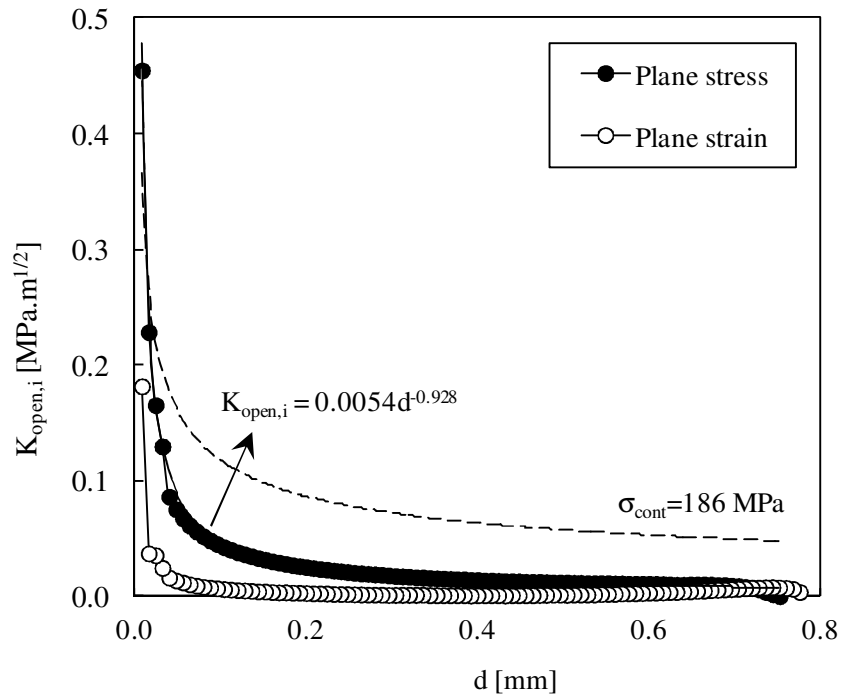


Figure 7. Contribution to K_{open} along crack flank
 $(\sigma_{max}=47.5 \text{ MPa}; a=5.9 \text{ mm}, \Delta K=6.5 \text{ MPa}\cdot\text{m}^{1/2}; R=0.02)$

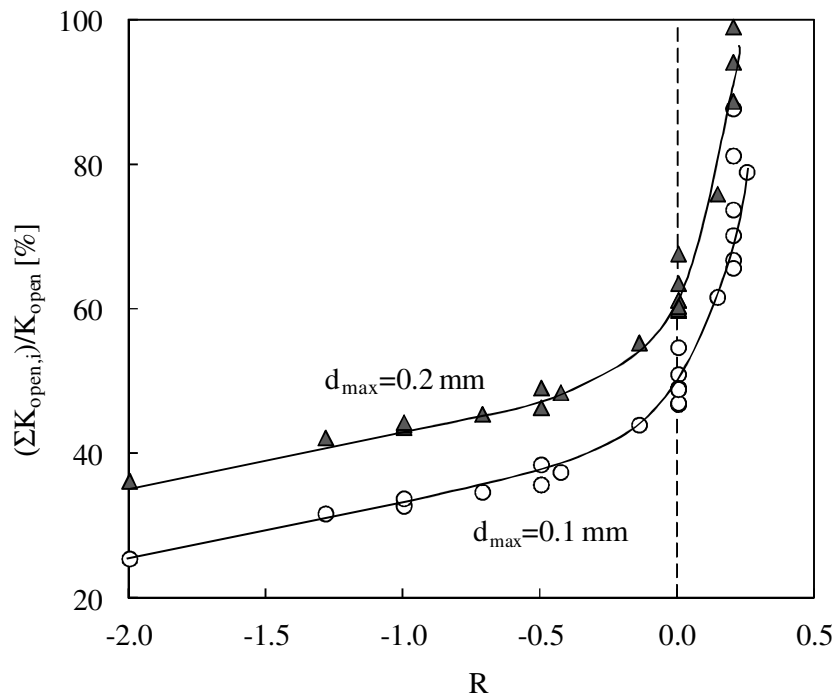


Figure 8. Cumulative stress intensity factor up to a distance d from crack tip (plane stress).

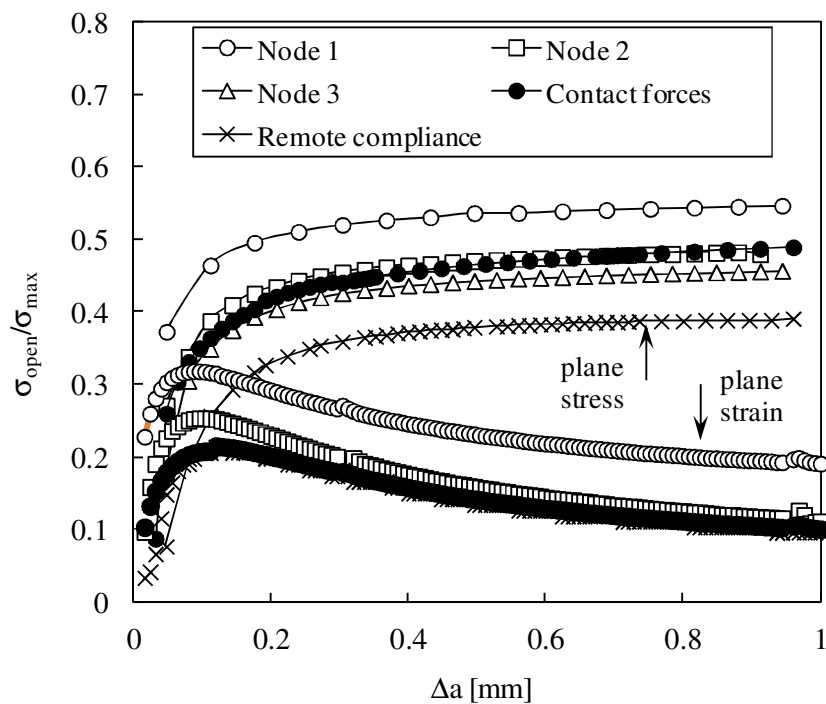


Figure 9. PICC versus crack increment
($L_1=8 \mu\text{m}$; $\sigma_{\text{max}}=47.5 \text{ MPa}$; $\sigma_{\text{min}}=0.83 \text{ MPa}$, plane stress).

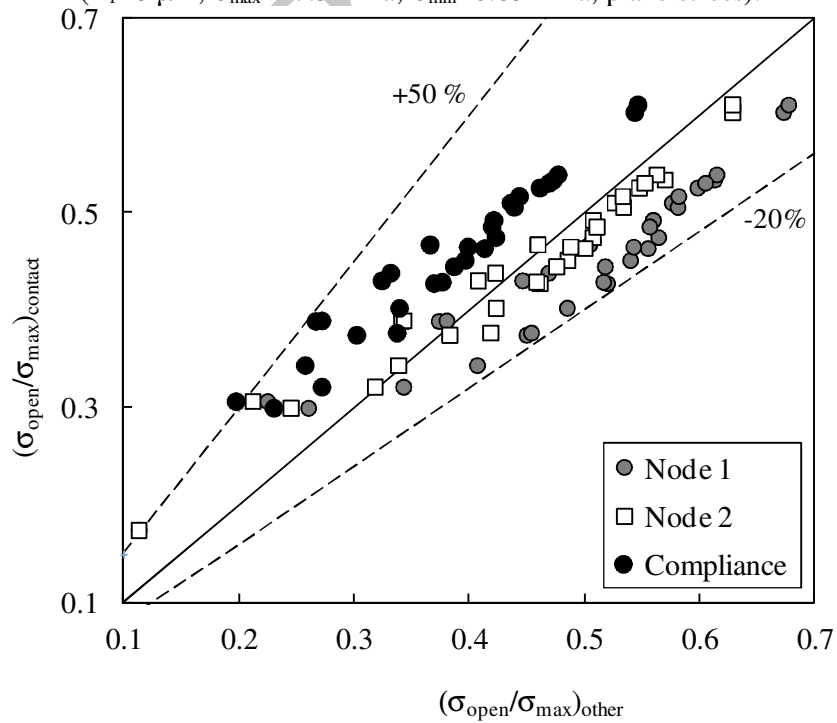


Figure 10. Comparison between different PICC parameters ($L_1=8 \mu\text{m}$, plane stress).

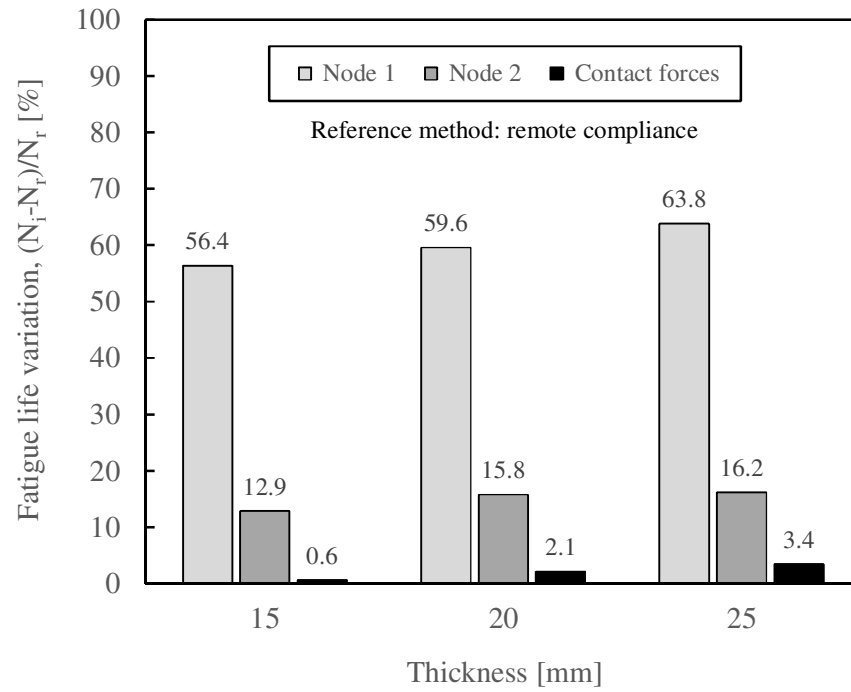


Figure 11. Comparison of fatigue lives obtained with different closure values.

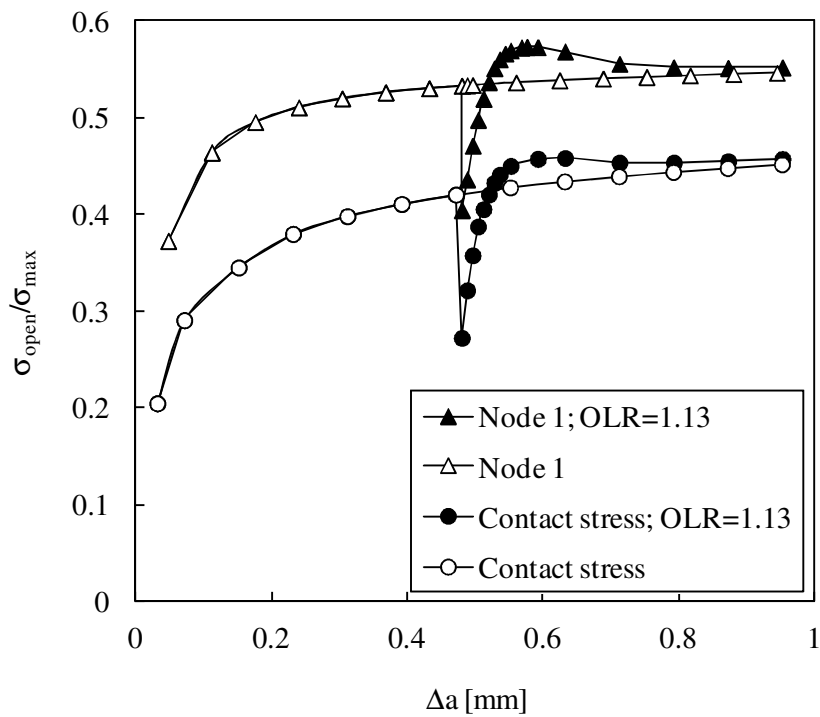
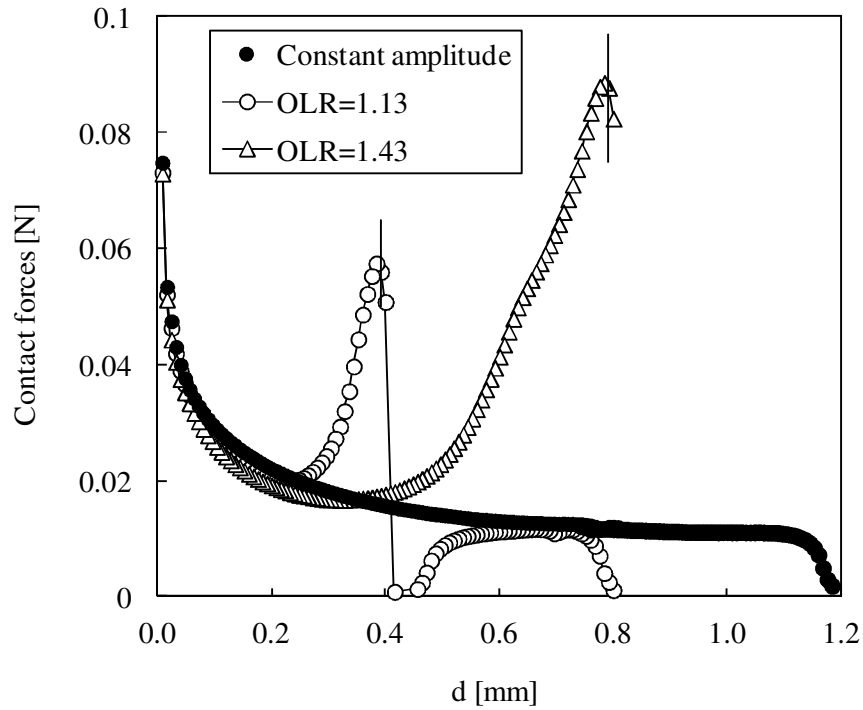


Figure 12. Effect of overloads ($OLR = \sigma_{ol} / \sigma_{max}$). a) Contact forces; b) PICC versus crack increment. (Plane stress; $L_1 = 8 \mu\text{m}$; $\sigma_{max} = 47.5 \text{ MPa}$; $R = 0$).

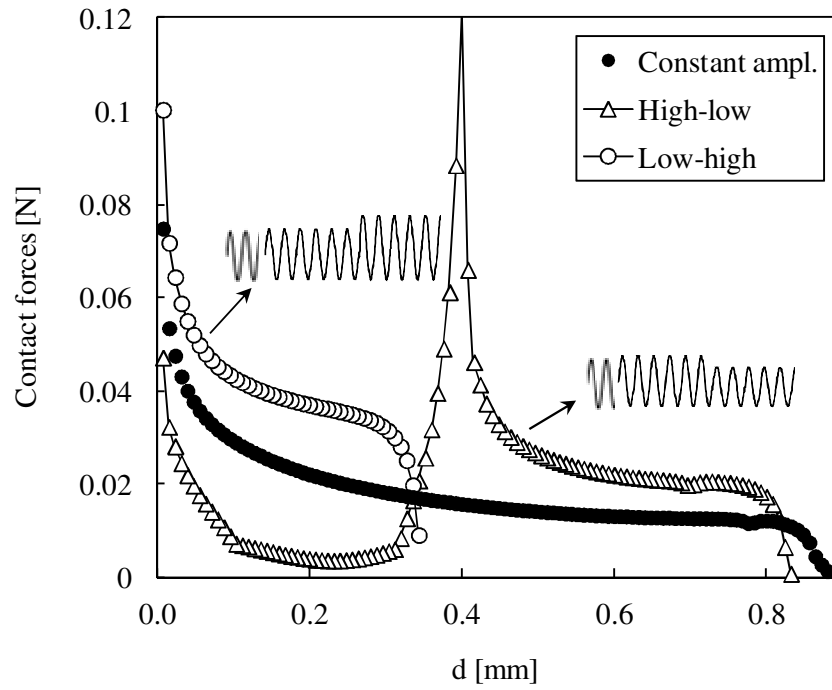


Figure 13. Effect of load blocks on contact forces (Plane stress; $L_1=8 \mu\text{m}$; $R=0.02$, $\sigma_{\max 1}=47.5 \text{ MPa}$, High-low: $\sigma_{\max 2}=36.7 \text{ MPa}$; Low-high: $\sigma_{\max 2}=60 \text{ MPa}$)

Table 1. Load parameters ($[\Delta K]$, $[K_{\max}] = \text{MPa} \cdot \text{m}^{1/2}$)

Set 1		Set 2		Set 3		Set 4		Set 5	
$(K_{\min}=0)$		$(K_{\max}=6.4)$		$(\Delta K=4.6)$		$(\Delta K=6.4)$		$(R=0.2)$	
ΔK	R	ΔK	R	ΔK	R	ΔK	R	ΔK	R
2.7	0	3.6	0.43	4.6	-2	6.4	-2	2.9	0.2
3.6	0	5.5	0.14	4.6	-1	6.4	-1	3.6	0.2
4.6	0	7.3	-0.14	4.6	-0.5	6.4	-0.5	4.4	0.2
6.4	0	9.1	-0.43	4.6	0	6.4	0	5.1	0.2
8.2	0	10.9	-0.71	4.6	0.25	6.4	0.25	5.8	0.2
9.1	0	12.8	-1.00	4.6	0.5	6.4	0.5	6.6	0.2
10.0	0	14.6	-1.29						

Table 2. Fitting constants of K^* versus d^* (equations 5-7).

		C_1	C_2
Plane stress	$d^* \leq 0.012$	0.4389	0.5096
	$0.012 < d^* \leq 0.2$	2.2490	0.4043
Plane strain	$d^* \leq 0.012$	0.3556	0.5091
	$0.012 < d^* \leq 0.2$	1.8161	0.3701

Table 3. Closure parameters used in FCG simulations.

	Node 1	Node 2	Remote compliance	Contact forces
U_A	0.45	0.50	0.59	0.54
U_B	0.69	0.76	0.79	0.79